

SmartLog: Metrics-driven Role Assignment for Byzantine Fault-tolerant Protocols

Hanish Gogada
University of Stavanger
Norway

Christian Berger
Friedrich-Alexander-Universität
Erlangen-Nürnberg
Germany

Leander Jehl
University of Stavanger
Norway

Hans P. Reiser
Reykjavik University
Iceland

Hein Meling
University of Stavanger
Norway

Abstract

Byzantine Fault Tolerant (BFT) protocols play a pivotal role in blockchain technology. As the deployment of such systems extends to wide-area networks, the scalability of BFT protocols becomes a critical concern. Optimizations that assign specific roles to individual replicas can significantly improve the performance of BFT systems. However, such role assignment is highly sensitive to faults, potentially undermining the optimizations' effectiveness. To address these challenges, we present SmartLog, a logging framework for collecting and analyzing metrics that help to assign roles in globally distributed systems, despite the presence of faults. SmartLog presents local measurements in global data structures, to enable consistent decisions and hold replicas accountable if they do not perform according to their reported measurements. We apply SmartLog to Kauri, an optimization using randomly composed tree overlays. SmartLog finds robust and low-latency tree configurations under adverse conditions.

1 Introduction

Byzantine Fault Tolerant (BFT) consensus protocols enable distributed systems that can tolerate arbitrary failures, making them a critical component for blockchain systems that distribute trust among participants that validate transactions and maintain the ledger. Therefore, to reduce reliance on a few participants and bolster security, scaling BFT protocols beyond their traditional capacity [13, 36] has become crucial.

Numerous studies have tackled the scalability challenges using various optimization strategies effective under specific favorable conditions [12, 21, 23, 42, 49]. However, in adverse scenarios, these optimizations become less effective or even defunct, necessitating a switch [5, 7] to a more resilient but less effective protocol, like PBFT [13], to make progress. It is, however, non-trivial to detect whether or not the operating conditions are favorable or adversarial. Existing work utilizes inefficient techniques based on randomness [21, 38, 42] or predefined assignments [49], requiring repeated trial-and-error to find a working system configuration. These systems often ignore the actual operating conditions, such as the latency between replicas and prior misbehavior, resulting

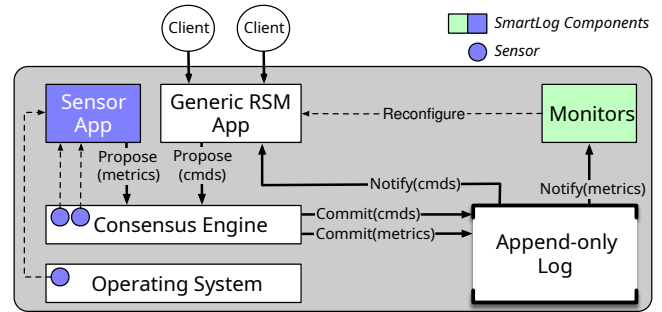


Figure 1. SmartLog's component architecture.

in poor performance. Many systems [8, 11, 19, 40, 43] that consider the operating conditions rely only on local measurements to select a system configuration. This is problematic because local measurements across the replicas may be inconsistent, making it challenging to make global configuration decisions. Similarly, there is a lack of transparency and trust if a single replica, e.g., the leader, can make such decisions based only on its local measurements since it is impossible to verify that the decision was based on actual measurements.

This paper advocates for a holistic, measurement-based approach to accurately identify the current operating conditions, promoting aggressive use of efficient protocols and reducing fallback to less efficient ones. We accomplish this through a shared append-only log of measurements.

We describe SmartLog, an integrated shared log for recording various metrics and computing efficient system configurations from these metrics. SmartLog extends a generic Replicated State Machine (RSM) with sensors and monitors to capture and evaluate different metrics. Individual replicas instrumented with sensors record measurements in the log, and corresponding monitors at replicas collate these measurements to derive *efficient configurations*. SmartLog enables replicas to make consistent configuration decisions based on the same information. The log also provides transparency, allowing all replicas to verify decisions and recognize faulty behaviors. Fig. 1 illustrates SmartLog's architecture; see §4 for a detailed description.

Moreover, some optimization techniques can be costly to (deterministically) evaluate for large configuration sizes. Thus, SmartLog allows heuristic optimization techniques to be used, where the resulting non-deterministic configurations are logged, such that the replicas can consistently determine a global ranking of configurations. SmartLog also supports collaborative optimization techniques where the search space is partitioned and distributed across the RSM replicas.

To showcase SmartLog’s effectiveness, we focus on BFT systems [34, 35, 42] that organize their RSM replicas in a tree topology for improved scalability. A tree topology reduces communication overhead by limiting interactions to parent and child replicas. However, this structure is vulnerable to failures, which can fragment the network. To counter this, tree-based protocols require fallback and reconfiguration mechanisms. Kauri [42], for example, builds multiple randomized trees to prevent targeted attacks, switching to a new tree when failures occur. However, this approach can cause considerable delays in reaching consensus due to the number of reconfigurations needed to find a working tree. Moreover, blindly constructing trees based on randomness can result in latency-imbalanced trees that degrade the RSM’s performance. Ideally, trees should be constructed with reliable replicas at the core and less reliable ones at the leaves.

Our second contribution, SmartTree, is a novel RSM optimization strategy that leverages SmartLog to collect metrics based on historical system behavior and performance. SmartTree is a heuristic tree selection algorithm designed to create low-latency trees while excluding faulty replicas from the tree’s core. Each replica uses simulated annealing [32] to search for a low-latency tree. Since simulated annealing is non-deterministic, the resulting trees are recorded in the log. From this logged data, replicas can deterministically select the tree with the lowest cumulative latency. SmartTree can reconfigure the RSM until a working tree is found, while recording the measurements in the log. This approach is guaranteed to find a working tree within at most $2f$ reconfigurations for certain tree configurations, where f is the maximum number of faulty replicas.

The main contributions of this paper are:

1. SmartLog, a logging framework for systematic metrics collection and configuration optimization for RSMs.
2. SmartLog enables RSM optimizations to compute heuristic configurations while maintaining accountability.
3. SmartTree uses SmartLog to generate low-latency working trees with linear reconfigurations.

2 Preliminaries

We consider an RSM that accepts client commands as input and produces output to clients. The RSM may record certain events in an append-only log. We assume an RSM with $n \geq 3f + 1$ replicas, where up to f can be Byzantine faulty,

meaning they may exhibit arbitrary, potentially adversarial behavior. Replicas that faithfully follow the protocol and do not crash are considered *correct*, while others are deemed *faulty*. In every view, at least a quorum of $q = n - f$ correct replicas is assumed to be available.

We assume a *partially synchronous* network [17], where periods of instability may cause unpredictable delays. However, after a *global stabilization time* (GST), latencies become predictable. We also assume there exists a known parameter δ and an *actual* latency $L_a(A, B)$ between correct replicas A and B , such that after GST, the round-trip time of any message between A and B is in the interval $[L_a(A, B), \delta \cdot L_a(A, B)]$.

Note that the partial synchrony assumption only pertains to liveness; the RSM’s safety is always preserved. A faulty replica may attempt to disrupt the RSM’s performance by recording incorrect measurements in the log. However, an adversary cannot delay messages, including measurements, between correct replicas. Thus, faulty replicas cannot interfere with measurement exchanges between correct replicas.

Let Π denote the set of n replicas constituting the RSM’s full *configuration*. A configuration also encodes topology information, e.g., a tree configuration. While describing the position of the replica in a tree/graph, it may also be referred as *node*. An RSM may *reconfigure* from one configuration to another, e.g., to activate a better configuration or recover from a faulty configuration.

3 Motivation

If you can’t measure it, you can’t improve it.

—Lord Kelvin

This section outlines several challenges with existing systems that motivate SmartLog’s design.

Manual performance tuning. Optimizing the performance of RSM-based protocols necessitates precise tuning to the conditions of their deployment environment. Performance parameters—such as the replication degree, batch size, concurrency, shard count, and network timeouts—must be carefully calibrated to balance efficiency and reliability. For instance, RSMs operating over wide area networks with inherently higher and less predictable latencies require more conservative timeouts compared to those on local area networks [20, 51]. For leader-based protocols, choosing a short timeout may lead to consecutive leader changes [38], while a longer timeout results in slower recovery from failures. A single leader often becomes a performance bottleneck [33, 50], and rotating the leader-role [53] can result in significant performance degradation when some replicas are faulty [22, 38]. Despite these challenges, the prevalent practice of manual performance tuning is fraught with complexities [2], often due to inadequate feedback mechanisms, resulting in configurations that are less than ideal.

Limitations of local-only measurements. Local measurements [8, 11, 19, 40, 43], where individual replicas capture

and use metrics without sharing this information with their counterparts, present inherent limitations. Such local-only observations can lead to discrepancies, as replicas might draw inconsistent conclusions about their operating environment. Furthermore, replicas cannot be held accountable for their configuration decisions based on local measurements as they are not verifiable by other replicas.

We don’t measure enough. RSM-based production systems use telemetry frameworks [12, 21] to collect various metrics such as latency, throughput, CPU and memory load, and so on. These metrics are typically used for offline analysis to understand and improve the RSM’s behavior under various workloads and network conditions. However, it is less common for these metrics to be used as input to real-time automated reconfiguration, e.g., to optimize the RSM’s operational performance. Such optimization hinges on accurate and agreed-upon measurements.

Measurement-based role assignment. A wide range of strategies exists for RSM optimization [10] and analysis, including pipelining [23, 26], committee selection [25, 30, 54], hierarchical consensus [34, 42], and forensics [47]. Typically, these optimizations rely on special roles, like coordinators, validators, or committee members. Conventionally, these roles are assigned in a randomized [21, 42] or predefined fashion [4, 39, 49], requiring trial-and-error to find a working assignment. This precludes informed decisions and learning from past configuration failures. Others use an external service [1, 24, 29], which may pose a single point of failure and does not align with the BFT trust model. Assignment based on measurements and prior experience is promising but requires an infrastructure to record measurements and decisions and draw conclusions. Moreover, the infrastructure must be suitable for the BFT trust model and sufficiently flexible to support a variety of optimization strategies.

Collaborative optimization. Optimizing RSM configurations often involves exploring a vast search space, and centralizing this task at a single replica leads to performance bottlenecks. A better solution is partitioning the search space into smaller tasks and distributing them across the replicas using scatter-gather [45] or map-reduce [15, 56] techniques. Despite their potential, these methods are surprisingly underutilized for optimizing RSM configurations.

Random configuration decisions are bad. Given a set of replicas which are deployed across the world, any two randomly selected configurations can have huge variance in performance. The distribution of the configuration latencies can be non-uniform, and the performance of the RSM can be significantly impacted by the configuration decision. The possibility of randomly selecting a bad configuration is high therefore choosing a random configuration is not a good idea.

Non-deterministic configuration optimization. Finding an effective configuration can be framed as a combinatorial optimization problem. Due to the vastness of possible

configurations, finding an optimal solution is often unfeasible. This makes heuristic approaches, including machine learning, more viable than deterministic methods. However, due to the inherent non-determinism of these heuristic solutions, existing systems [9] do not support non-deterministic configuration optimization.

4 SmartLog Architecture Overview

This section gives an overview of SmartLog’s architecture, as shown in Fig. 1. SmartLog offers measurement and monitoring facilities to optimize various aspects of a generic RSM application, such as its performance and scalability. The RSM uses a *consensus engine* to consistently replicate client commands to an *append-only log*. Optimizing the RSM requires metrics on both its state and environment. To achieve this, SmartLog augments each replica with *sensors* and *monitors*. These components use the log to share information about the system’s configuration and sensor metrics with all replicas.

Sensors collect various metrics and pass them to the *sensor app*, which uses the consensus engine to disseminate authenticated sensor metrics to all replicas. These metrics can come from different sources, such as the replica’s operating environment or sensors integrated into the consensus engine. The monitors act as counterparts to sensors, receiving notifications about specific metrics.

Fig. 2 shows how monitor M_1 (M_2) collect metrics from sensor S_1 (S_2) at replicas A , B , C , and D . Since these metrics are committed to the log, monitors can build a consistent global view of the environment. This allows SmartLog replicas to make operational decisions based on deterministic information rather than local-only sensor data. As shown in Fig. 2, monitor M_2 makes reconfiguration decisions for the RSM based on globally recorded and agreed-upon metrics. For example, one of our monitors generates a latency matrix that provides insights into the latencies between all participating replicas, as discussed in §4.1.1.

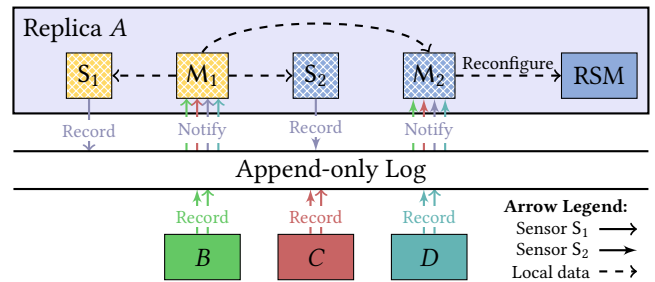


Figure 2. Replicas (A, B, C, D) with sensors and monitors.

4.1 Sensors and Monitors

This section presents SmartLog’s mechanisms for collecting and processing metrics, namely sensors and monitors. Each

sensor-monitor pair has a one-to-one relationship, as shown with S_1-M_1 and S_2-M_2 in Fig. 2.

A *sensor* abstracts the capture of local-only metrics related to a replica’s operational context. Sensors can be integrated into system components, such as the consensus engine, or can query the operating system for metrics such as CPU load. A sensor can also use information from local monitors, as exemplified by the dashed arrow from M_1 to S_1 in Fig. 2. A sensor’s output is assumed to be non-deterministic and may vary across replicas. Sensors may also perform non-deterministic computations, e.g., to support heuristic and distributed optimization algorithms. We refer to both sensor output and compute results as *measurements*. These measurements are recorded in the log, providing a consistent record of the system’s operation. The recorded measurements are later accessed by monitors, as discussed below.

In a Byzantine environment, sensors at up to f faulty replicas may report incorrect measurements. Consequently, any monitor using these measurements must account for potential inaccuracies. Despite this, retaining a record of incorrect measurements can be invaluable for forensic analysis.

The *monitor* is the core abstraction linking sensor measurements from individual replicas with system-wide operations, enabling dynamic adjustments to the RSM. When a sensor records a measurement, the corresponding monitor updates its data structures through the following steps:

1. **Data Collection:** The monitor collects metrics from its associated sensor via the log and may also use data from other local monitors.
2. **Deterministic Computation:** The monitor processes collected metrics into consistent data structures.

Since monitors on each replica operate on the same ordered set of measurements, they maintain consistent data structures across the system. This consistency provides a consolidated, global view of the measurements, allowing replicas to coordinate system-wide operations reliably, such as activating a new tree configuration with SmartTree (§5). Table 1 summarizes the key properties of sensors and monitors.

Table 1. Summary of sensor and monitor properties.

Property	Sensors	Monitors
Input	System & local monitors	Log & local monitors
Computation	Non-deterministic	Deterministic
Output	Variable across replicas	Consistent across replicas

In the following sections we present the sensors and monitors we implemented for SmartLog, and Fig. 3 shows how these interact to ensure robust configurations.

4.1.1 Latency Monitoring. We now discuss our approach to measuring latencies between replicas in a star topology.

We measure the *round-trip latency* of protocol message exchanges. Our LatencySensor instruments the consensus

engine’s Proposal-Vote exchange, capturing the latency between the proposing (leader) replica and the voting replicas. The leader then compiles these latencies into a *latency vector*, which is included in the next proposal. Any faulty replicas that did not vote are marked as ∞ in the latency vector. To collect measurements from each replica’s vantage point, we assume frequent leader rotation (views), a common practice in star topologies.

Each replica has a LatencyMonitor that maintains a *latency matrix* L , representing inter-replica latencies. When a proposal is committed, the monitor updates the leader’s row in L based on the proposal’s latency vector. To maintain a symmetric matrix, we set $L_{A,B} = L_{B,A} = \max(L_r(A, B), L_r(B, A))$, where $L_r(A, B)$ is the *recorded* latency between replicas A and B . To allow all replicas to build a complete latency matrix, at least $2n$ views are needed. The monitor may repeat this process to improve L ’s accuracy.

In a Byzantine environment, L may not accurately reflect inter-replica latencies. We now examine scenarios where replicas record incorrect measurements to distort the matrix.

Scenario	Recorded vs Actual Latency
1: A and B are non-faulty	$L_{A,B}$ in $[L_a(A, B), \delta L_a(A, B)]$
2: A or B is faulty	$L_{A,B} \geq (\leq) L_a(A, B)$
3: A and B are faulty	$L_{A,B} \geq \text{or } \leq L_a(A, B)$

In Scenario 1, A and B are correct, so their recorded latency matches the actual latency. In Scenario 2, the L at correct replicas reports the highest latency. Thus, $L_{A,B} < L_a(A, B)$ is unlikely when either A or B is faulty. For a faulty replica to log a latency lower than the actual value, it would need to collude with another replica C that has a lower latency to the correct replica. However, to benefit from C ’s lower latency, the faulty replica needs to synchronize with C , which may itself add latency and make this strategy difficult. We do not assume that such cases cannot happen, but consider them unlikely. In Scenario 3, both replicas are faulty, so we ignore their L entries as meaningless.

Our latency measurement technique offers three key benefits over existing methods [6, 9, 11]. First, it measures actual protocol latency, including command execution, rather than just network latency experienced by dummy messages. Second, it supports incremental logging, allowing extended data collection and refinement. Finally, we can use historical latency data for more thorough analysis to improve accuracy and reliability.

4.1.2 Misbehavior Monitoring. A significant challenge for scalable RSMs is to stay optimized despite faulty replicas disrupting the configuration. SmartLog provides two monitors for detecting faulty replicas: one precise (this section) and one for suspicions (§4.1.3).

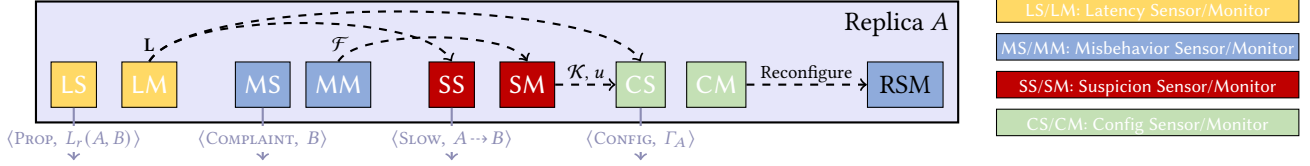


Figure 3. Connections between Replica A’s sensors and monitors.

Precise detection is possible using the *proof-of-misbehavior* technique [3, 16, 27, 36, 46]. The MisbehaviorSensor, integrated into the consensus engine, observes the replicas’ protocol-specific behavior and raises a *complaint* when detecting a provable violation. Complaints are signed and proposed via the sensor app and logged. Detected misbehaviors include invalid threshold signatures, proposals, votes, complaints, and equivocation. An equivocation is identified when replicas detect the leader sending different messages, when the protocol dictates that it should have sent the same message.

When a complaint proposal is received, each replica’s MisbehaviorMonitor verifies its validity. If valid, the monitor updates its *list of provably faulty replicas* \mathcal{F} , which can be used to exclude them from special protocol roles, such as leader.

4.1.3 Suspicion Monitoring. Gathering enough evidence to substantiate a proof-of-misbehavior complaint against a replica is often impossible. Therefore, we introduce suspicion monitoring to detect timing and omission faults. These suspicions are processed to produce a candidate set that avoids suspected replicas.

The SuspicionSensor is embedded in the consensus engine, allowing it to monitor both replies and view timeouts. It raises suspicions on (a) slow replicas, (b) slow leaders, and (c) replicas issuing false suspicions. Let $A \leftrightarrow B$ denote that A suspects B . The sensor at replica A logs a suspicion message whenever condition (a), (b), or (c) is met, as outlined below.

Condition for Suspicion	Timeout	Suspicion
(a) No response from B within timeout	$\delta \cdot L_{A,B}$	$\langle \text{SLOW}, A \leftrightarrow B \rangle$
(b) View with leader L timed out	$\delta \cdot \max_{V \in \Pi} L_{L,V}$	$\langle \text{SLOW}, A \leftrightarrow L \rangle$
(c) False suspicion from B on A		$\langle \text{FALSE}, A \leftrightarrow B \rangle$

First, $A \leftrightarrow B$ if B fails to respond within a timeout of $\delta \cdot L_{A,B}$, where $L_{A,B}$ is the latency reported by the LatencyMonitor. This mechanism ensures that omission failures also lead to suspicion. Second, $A \leftrightarrow L$ if A does not receive a proposal message within the view timeout. The view timeout is also adjusted based on latencies from the LatencyMonitor. However, since the leader must wait for slower replicas before responding, the view timeout is based on the maximum latency in the leader’s row. Finally, if a $\langle _, B \leftrightarrow A \rangle$ is raised, A reciprocates by raising a $\langle \text{FALSE}, A \leftrightarrow B \rangle$.

After GST, no two correct processes will raise suspicions against each other. This holds because the latencies between correct replicas have stabilized, and latency measurements and timeouts have been adjusted accordingly.

To produce a candidate set, the SuspicionMonitor first removes provably faulty replicas \mathcal{F} , reported by the MisbehaviorMonitor. Next, the SuspicionMonitor distinguishes between crash suspicions and misbehavior suspicions. It then filters out certain suspicions raised by misbehaving replicas to prevent a single Byzantine replica from excluding many correct replicas. The monitor then outputs a candidate set of replicas considered correct, along with an estimate of the number of misbehaving replicas.

Condition (c) allows us to distinguish suspicions against crashed replicas from those caused by misbehaving replicas. A crashed replica B will be suspected by others through $\langle \text{SLOW}, A \leftrightarrow B \rangle$. If a faulty replica B raises $\langle \text{SLOW}, B \leftrightarrow A \rangle$ against a correct replica A , then A will reciprocate with $\langle \text{FALSE}, A \leftrightarrow B \rangle$. Thus, a replica suspected of being slow without raising a counter-suspicion is *considered crashed*. Conversely, if two replicas suspect each other, it remains unclear which one is faulty. The SuspicionMonitor maintains separate data structures for these two cases, a set \mathcal{C} for crashed replicas, and a graph \mathcal{G} for other suspicions. Formally, $\mathcal{G} = (\mathcal{V}, \mathcal{E})$ is an undirected graph where the vertices $\mathcal{V} = \{\Pi \setminus \mathcal{F} \setminus \mathcal{C}\}$ represent possible candidate replicas, and an edge $(A, B) \in \mathcal{E}$ indicates a two-way suspicion, $A \leftrightarrow B$.

When a suspicion $\langle \text{SLOW}, A \leftrightarrow B \rangle$ is raised against a correct replica B , it may take several views before a reciprocation $\langle \text{FALSE}, B \leftrightarrow A \rangle$ is logged, especially if faulty replicas attempt to censor such suspicions. We therefore treat every new suspicion between two replicas in \mathcal{V} as a two-way suspicion by adding the corresponding edge to \mathcal{G} . If no reciprocation is received within $f + 1$ leader changes (views), the edge is treated as a one-way suspicion, and B is added to \mathcal{C} .

The SuspicionMonitor computes a maximum independent set from the vertices in \mathcal{G} and uses it as the candidate set \mathcal{K} . This computation must be deterministic, to ensure that all correct replicas reach the same conclusion. Additionally, the monitor outputs the estimated number of misbehaving replicas, $u = |\mathcal{V}| - |\mathcal{K}|$.

Before GST, unstable latencies may cause suspicions, even between correct replicas. To prevent these suspicions from persisting indefinitely, the SuspicionMonitor employs two mechanisms. First, if the system remains stable with no new

suspicions for w views, the monitor begins removing old suspicions in the order they appear in the log. Second, if too many suspicions are received, it also starts discarding old suspicions. Too many suspicions occur when \mathcal{G} no longer contains an independent set of size $n - f$.

4.1.4 Configuration Monitoring. SmartLog’s monitoring architecture is also used to trigger reconfigurations. The ConfigSensor searches for a new configuration and proposes it via the log. The ConfigMonitor then selects among the proposed configurations and initiates reconfiguration.

This separation has several benefits. First, while the monitor’s reconfiguration decision must be deterministic and taken by all replicas, the sensor’s search for a better configuration can be performed by a single replica. Second, when the search space is large, the sensor can use more efficient non-deterministic search algorithms. Lastly, the search space can be divided among the replicas.

The ConfigSensor utilizes measurements from other monitors to find a new configuration. A search can be triggered periodically, by a significant change in another monitor’s output, or by specific events like view failures. Typically, the ConfigSensor relies on the SuspicionMonitor and MisbehaviorMonitor to exclude *invalid configurations*, such as those involving a crashed leader. The remaining configurations are ranked using a scoring function, and the best-scoring configuration, Γ , is proposed to the log. In our example, the scoring function predicts the configuration’s latency using L from the LatencyMonitor. Other scoring functions are possible, such as those that optimize throughput based on CPU and network utilization.

When the ConfigMonitor receives a configuration proposal Γ , it first checks that the proposal represents a *valid configuration*. The monitor also checks if the current configuration has become invalid, e.g., due to an updated \mathcal{K} from the SuspicionMonitor. If the current configuration is invalid, reconfiguration is needed. However, the monitor waits for at least $f + 1$ replicas to propose new configurations before selecting the one with the best score. This prevents reconfiguring to a potentially suboptimal configuration proposed by a faulty replica. The monitor can trigger a reconfiguration even if the current configuration is still valid but has been active for a while. In which case, the monitor requires the new configuration to have a significantly better score to avoid frequent reconfigurations that could disrupt the system.

5 SmartTree

This section introduces SmartTree, a variant of Kauri [42], utilizing SmartLog to construct correct, low-latency trees.

5.1 Preliminaries for SmartTree

5.1.1 A Brief Primer on Kauri. This section gives an overview of Kauri and its reconfiguration approach. To improve scalability, Kauri replaces HotStuff’s star topology

with a tree topology (Fig. 4), where leader R disseminates proposals top-down and aggregates votes bottom-up. We refer to replicas with a specific role or placement in the tree as nodes. In this structure, Kauri’s *internal nodes*, $\mathcal{I} = \{R, I_1, \dots, I_b\}$, manage only b child nodes, where b is the tree’s branch factor. As a result, the internal nodes experience a much lower load than HotStuff’s leader, which must interact with $n - 1$ replicas. Let $\mathcal{M} = \mathcal{I} \setminus \{R\}$ denote the *intermediate nodes*, and $\mathcal{L} = \Pi \setminus \mathcal{I} = \{T_1, \dots, T_{b^2}\}$ the *leaf nodes*.

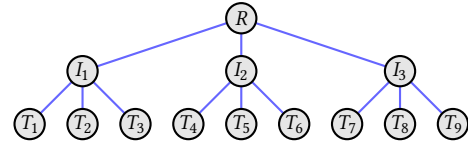


Figure 4. Tree with $n = 13$ replicas and branch factor $b = 3$.

Kauri exploits the parallelism of its tree topology through pipelining. Specifically, the root can initiate multiple consensus instances concurrently, resulting in higher throughput than a comparable star topology.

However, it is hard to construct trees in the presence of faults. That is, the internal nodes of a tree can control both the dissemination and aggregation stages of the protocol. In a star topology, assuming an honest leader, protocol execution may succeed despite some faulty votes. This may not be the case for a tree topology. To address this concern, Kauri forms a correct tree using a reconfiguration algorithm based on t -Bounded Conformity [42]. This method involves dividing the replicas into t disjoint bins, assuming that $f < t$, where $t = n/i$ and i is the number of internal nodes. Kauri then constructs trees using these bins, with replicas in each bin serving as internal nodes and the rest as leaf nodes. If $f < t$, there is always at least one fault-free bin, ensuring at least one tree with correct internal nodes. If Kauri is unable to establish a correct tree within t reconfiguration trials, it reverts to using a star topology. Neiheiser et al. [42] show that a three-level tree can guarantee liveness if the internal nodes are correct. Their reconfiguration algorithm exploits this guarantee by iterating through trees constructed from disjoint sets of internal nodes.

5.1.2 Kauri’s Challenges. In a wide-area environment, Kauri may face several challenges: 1) A single faulty replica may exclude many other replicas from being considered as internal nodes. Moreover, if latencies are not uniform, the performance of successive trees may degrade significantly. 2) Kauri reconfigures only when a tree fails to collect q replies. For example, if a low-latency subtree fails, Kauri may wait for a higher-latency subtree to respond, resulting in degraded performance. 3) Kauri’s reconfiguration approach only supports $\mathcal{O}(\sqrt{n})$ reconfigurations.

To address Challenge 1, SmartTree eliminates faulty replicas from the candidate set, individually or paired with at

most one correct replica. For Challenge 2, SmartTree dynamically adjusts the tree’s failure threshold based on recorded suspicions. Further, we prove that in any scenario with up to f faults, SmartTree uses at most $2f$ reconfigurations to find a correct tree, addressing Challenge 3.

5.2 Overview of SmartTree

SmartTree’s goal is to find correct, low-latency trees for large-scale RSM deployments. A *correct tree* is one where the internal nodes are correct, ensuring that the tree can collect a quorum of votes. However, an arbitrary correct tree may be suboptimal, and so SmartTree additionally aims to minimize the tree’s latency based on the replicas’ recorded latencies. We define *tree latency* as the time it takes for the root to disseminate the proposal and aggregate a quorum of votes. A tree fails when it cannot collect a quorum of votes within a timeout. In the following, we explain how SmartLog’s sensors and monitors are adjusted to match the characteristics of a tree topology.

5.3 SmartTree Monitors

This section describes how we adjust the existing sensors and monitors to work with tree topologies.

First, we do not record latencies while the RSM is in a tree configuration. This is because the tree structure prevents direct communication between replicas, making it difficult to measure individual latencies. Instead we measure latencies only in a star topology. Thus, we do not need to adjust the latency monitoring for trees. At first glance, this lack of recorded tree latencies may seem like a weakness that an adversary could exploit. A Byzantine replica may initially behave correctly in order to be selected as an internal node. However, if it later misbehaves, e.g., by delaying messages, it will be suspected by the suspicion monitor, resulting in a failed tree. When a tree fails, the replicas revert to the star topology to record new measurements. In §5.3.1, we adapt the configuration sensor to search for efficient trees. In §5.3.3, we modify the suspicion sensor to detect slow behavior in the tree overlay. We also optimize the suspicion monitor to compute a candidate set more efficiently, limiting the number of reconfigurations caused by faulty replicas.

5.3.1 Configuration Monitoring in Trees. Configuration monitoring in SmartTree is responsible for finding efficient tree configurations and activating the best one. As outlined in §4.1.4, the ConfigSensor may start a search periodically or when the current configuration is no longer valid. A tree configuration is valid if all internal nodes are part of the candidate set \mathcal{K} from the SuspicionMonitor. Thus, when a tree fails, SmartTree reverts to a star topology to record suspicions. Once these suspicions result in a change of \mathcal{K} , the ConfigSensor initiates a search for a new tree.

The ConfigSensor searches for a valid, low-latency tree using latencies \mathbf{L} from the LatencyMonitor and the candidate

set \mathcal{K} from the SuspicionMonitor. Additionally, the ConfigSensor uses the estimated number of misbehaving replicas u to search for a tree that provides low latency despite u many unresponsive leaves.

Since searching for optimal trees in large systems is intractable, we use a heuristic optimization technique based on simulated annealing [32]. To ensure that only valid trees are considered, internal nodes must be selected from \mathcal{K} . We initiate the search with a random tree, ensuring that internal nodes are only selected from \mathcal{K} . Simulated annealing uses a *mutate* function to randomly swap two nodes in the tree. Our mutate function ensures that internal nodes are only swapped with other nodes from \mathcal{K} .

Simulated annealing then compares the latency of the mutated tree with that of the best tree found so far and probabilistically selects the lower-latency tree for further mutation. The tree latency is computed using the scoring function in Definition 1 with parameter $k = q + u$. This score is the latency required to collect q votes from the tree, assuming that u leaf nodes are unresponsive. While simulated annealing allows exploration beyond local minima, it does not guarantee a global minimum. The search ends when the *search timer* expires or when simulated annealing converges. At this point, the ConfigSensor logs the lowest-latency tree found.

The ConfigMonitor waits for $f + 1$ valid tree configurations to be committed to the log and ranks them using the scoring function. It then selects the lowest-latency tree for reconfiguration.

Definition 1. For a tree τ , the *score*(k, τ) is the minimum latency required to collect votes from k nodes.

This score is computed using the link latencies in the tree, derived from \mathbf{L} , taking into account that intermediate nodes first collect votes from their children before forwarding them to the root.

The *aggregation latency* $L_{agg}(I)$, for intermediate node I , is the maximum latency from I to any of its children, $\text{Ch}(I)$:

$$L_{agg}(I) = \max_{V \in \text{Ch}(I)} \mathbf{L}_{I,V}$$

Let \mathcal{M}_k represent subsets of all intermediate nodes such that the subtrees rooted at these nodes contain a total of at least k nodes:

$$\mathcal{M}_k = \{M \subset \mathcal{M} \mid \sum_{I \in M} |\text{Ch}(I)| + 1 \geq k\}$$

Thus, the time to collect k votes is the minimum time to collect aggregates from subtrees in a set from \mathcal{M}_{k-1} , since the root R ’s vote is added separately.

$$\text{score}(k, \tau) = \min_{M \in \mathcal{M}_{k-1}} \left(\max_{I \in M} (L_{agg}(I) + \mathbf{L}_{I,R}) \right)$$

5.3.2 Misbehavior Monitoring in Trees. We augment misbehavior monitoring for trees with an additional rule for

invalid vote aggregation. In a tree configuration, intermediate nodes are responsible for aggregating votes from their children and forwarding them to the root. However, if an intermediate node does not receive a vote from a child node, the aggregate vote must include a suspicion for the missing vote. That is, the aggregate must include $b + 1$ votes or suspicions. Failure to meet this requirement allows the root to use the aggregation vote as *proof-of-misbehavior* against the intermediate node.

5.3.3 Suspicion Monitoring in Trees. The tree’s more complex communication pattern requires adjusting how suspicions are raised. Table 2 shows the adjusted conditions for raising suspicions in a tree configuration. In a star configuration (§4.1.3), the leader suspects replicas that fail to reply in time (a). In a tree, internal nodes suspect their children if they do not respond in time (Ta). However, the root’s timeout must also be adjusted to account for the time it takes the intermediate node to collect votes from its children (Ta’).

Similarly, in a star configuration, replicas suspect the leader upon a view timeout (b). In a tree configuration, we use the score of the configuration $score(q + u, \tau)$ as timeout, adjusted by δ . But only intermediate nodes directly suspect the root upon a view timeout (Tb). However, if faulty intermediate nodes prevent the root from collecting enough votes to advance the view, the root instead forwards suspicions to avoid being suspected. If a leaf does not receive a proposal, it could be caused by the root not sending the proposal or by the intermediate node failing to forward it. Therefore, leaf nodes do not immediately issue suspicions on view timeout; instead, they wait for the internal nodes to raise suspicions. If no such suspicion is raised, the leaf suspects both the root and the intermediate node (Tb’). Finally, correct replicas reciprocate suspicions raised by faulty replicas (c), as in the star configuration.

Table 2. Suspicion cases in a tree topology.

Condition for Suspicion	Timeout	Suspicion
(Ta) I : No response from T	$\delta \cdot L_{I,T}$	$\langle \text{SLOW}, I \rightarrow T \rangle$
(Ta’) R : No response from I	$\delta \cdot (L_{agg}(I) + L_{R,I})$	$\langle \text{SLOW}, R \rightarrow I \rangle$
(Tb) I : View timeout and no suspicion	$\delta \cdot score(q + u, \tau)$	$\langle \text{SLOW}, I \rightarrow R \rangle$
(Tb’) T : View timeout and no suspicion during	$\delta \cdot score(q + u, \tau)$	$\langle \text{SLOW}, T \rightarrow R \rangle$
(Tc) A : False suspicion from B	$\delta \cdot score(q + u, \tau)$	$\wedge \langle \text{SLOW}, T \rightarrow I \rangle$
		$\langle \text{FALSE}, A \rightarrow B \rangle$

When computing a maximum independent set for candidate selection (§4.1.3), a single intermediate node suspected by a leaf may cause the candidate set to update and require a reconfiguration. Faulty replicas may force $\Omega(f^2)$ reconfigurations before they are excluded from the candidate set [31].

We use a different approach to compute u and the candidate set \mathcal{K} for trees. This method produces smaller candidate

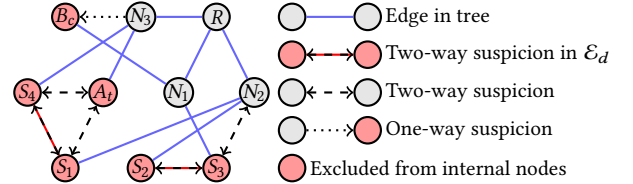


Figure 5. Example of suspicions leading to removal of nodes as candidates for internal tree positions.

sets and requires at most $2f$ reconfigurations, while avoiding the computational complexity of finding a maximum independent set.

We introduce two additional data structures, \mathcal{E}_d and \mathcal{T} , both derived from \mathcal{G} . \mathcal{E}_d is a maximal set of disjoint edges in \mathcal{G} . For every edge in \mathcal{E}_d , at least one of the adjacent vertices is a faulty replica. We therefore exclude both replicas from \mathcal{K} . Whenever an edge is added to \mathcal{G} , the suspicion monitor checks if \mathcal{E}_d is still maximal. This check includes possibly removing one edge from \mathcal{E}_d and adding two new ones. We also determine \mathcal{T} , the set of vertices that are not adjacent to an edge in \mathcal{E}_d but part of a triangle in \mathcal{G} with an edge in \mathcal{E}_d . We also exclude replicas in \mathcal{T} from \mathcal{K} .

Finally, we return \mathcal{K} containing replicas (vertices) in \mathcal{G} that are not in \mathcal{T} or adjacent to an edge in \mathcal{E}_d . We also return the estimated number of faulty replicas $u = |\mathcal{E}_d| + |\mathcal{T}|$.

Fig. 5 illustrates a suspicion graph \mathcal{G} and the resulting tree configuration with excluded nodes. In this example, $\mathcal{E}_d = \{(S_1, S_4), (S_2, S_3)\}$, as adding any other suspicion would violate the disjoint property of \mathcal{E}_d , which is already maximal. The set $\mathcal{T} = \{A_1\}$ includes nodes that form a triangle with one edge in \mathcal{E}_d and two others in \mathcal{G} . As B_c has a one-way suspicion, it is added to \mathcal{C} . Since we exclude all replicas (vertices) from \mathcal{T} , \mathcal{E}_d , and \mathcal{C} from the configuration Π making $\mathcal{K} = \{N_1, N_2, N_3, R\}$.

6 SmartTree Correctness

In this section, we proof correctness properties for SmartTree. SmartTree provides the following guarantees:

- C1 There are always enough candidates available to form a tree. (Theorem 6.1)
- C2 If a tree configuration fails and the system reverts to a star topology, sufficient suspicions will be recorded to update the candidate set and invalidate the failed tree configuration. (Lemma 1 & 2)
- C3 After GST, no two correct replicas raise suspicions against each other. (Lemma 3)
- C4 After GST, at most $2f$ reconfigurations are needed to form a correct tree. Specifically, if $t < f$ replicas are faulty, at most $2t$ reconfigurations are needed. (Theorem 6.2)

Faulty replicas can cast suspicions on non-faulty replicas to exclude them from being selected as internal nodes. However,

SmartTree can continue to form and reconfigure to new trees if there are enough candidate replicas to select the internal nodes. The process for selecting candidate internal nodes is detailed in Section 5.3.3. It involves constructing \mathcal{E}_d from the suspicion graph \mathcal{G} . [Theorem 6.1](#) shows that enough candidate replicas are always available to form a tree.

Theorem 6.1. *There are always enough candidate replicas available for selecting the internal nodes to form a tree.*

Proof. A tree configuration of size $n \geq 3f + 1$ with a branch factor $b \leq \sqrt{n}$ requires at most $\sqrt{n} + 1$ replicas as internal nodes. As explained in Section 4.1.3, the graph \mathcal{G} always contains an independent set (*IS*) of at least $n - f$ replicas. Then, we construct \mathcal{E}_d and \mathcal{T} from \mathcal{G} , where \mathcal{E}_d is a maximum set of disjoint edges and \mathcal{T} is a set of nodes that form a triangle in \mathcal{G} with an edge in \mathcal{E}_d . For any edge in \mathcal{E}_d , at most one of the two vertices is in *IS*. Since \mathcal{E}_d is disjoint, each vertex belongs to at most one edge in \mathcal{E}_d . Moreover, for any edge in \mathcal{E}_d that forms a triangle in \mathcal{G} , only one of the three vertices forming the triangle can be in *IS*.

Due to the maximality of \mathcal{E}_d , any edge in \mathcal{E}_d can be part of at most one triangle involving a replica in \mathcal{T} . Therefore, if at most f replicas are outside *IS*, the number of vertices in the independent set adjacent to edges in \mathcal{E}_d or in \mathcal{T} is at most f . Consequently, the remaining replicas in *IS* (at least $f + 1$) are available as candidates for internal nodes.

For $n \geq 13$, we have $\sqrt{n} < f$, implying that for configuration sizes of 13 and above, there are always enough candidate replicas available for selecting internal nodes. \square

Lemma 1. When a tree fails, either (1) one suspicion between internal nodes is raised, or (2) $u + 1$ leaves, not in \mathcal{C} get suspected.

Proof. A tree fails, if the replica at the root fails, or cannot collect $n - f$ votes in time. If the root fails, it is suspected by other internal nodes, matching (1) from the Lemma. Otherwise, the root waits for aggregates from internal nodes, which together aggregate more $n - f + u$ votes. Thus, there are two possibilities. Either at least $u + 1$ leaves are missing and suspected by their parents, matching (2), or one internal node is either missing or did send a faulty aggregate, and is suspected by the root, matching (1). \square

Lemma 2. If a tree failed, either: (i) $|\mathcal{E}_d|$ increases, or (ii) $|\mathcal{T}|$ increases and $|\mathcal{E}_d^n|$ stays unchanged.

Proof. All suspicions are added to the graph \mathcal{G} . In case (1) of Lemma 1, the new suspicion can be added to \mathcal{E}_d and \mathcal{T} remains unchanged. In case (2), $u + 1$ edges are added to \mathcal{G} . These new edges include $u + 1$ different leaves from the failed tree. These leaves, can be already adjacent to an edge in \mathcal{E}_d or part of \mathcal{T} . There are three cases: a) one leaf was not part of \mathcal{E}_d or \mathcal{T} . The new edge can be added to \mathcal{E}_d giving case (i) of the Lemma. b) one leaf was part of \mathcal{T} . The new edge can be added to \mathcal{E}_d and $|\mathcal{T}|$ is reduced by 1, giving case (i) of the

Lemma. (3) all leaves are part of \mathcal{E}_d , but since $|\mathcal{E}_d| \leq u$, at least two suspected leaves are already connected in \mathcal{E}_d . This allows to either replace one edge in \mathcal{E}_d by two new ones, or add a new node to \mathcal{T} . \square

6.1 Reconfiguration Proof

In the following, we show that SmartTree ensures that after GST, a working configuration is found after at most $2t$ reconfigurations, where t is the actual number of faulty replicas in the system, i.e. $t \leq f$. This is [Theorem 6.2](#).

We first proof [C3](#) as [Lemma 3](#).

Lemma 3. After GST, no two correct replicas suspect each other.

Proof. [Table 2](#) describes the conditions for raising suspicions in a tree. After GST, the round-trip time between two correct replicas A and B is in the interval $[L_a(A, B), \delta \cdot L_a(A, B)]$. It follows that no suspicions between A and B will be raised based on conditions (Ta). For (Ta') the same follows, since a correct intermediate node waits at most $\delta \cdot (L_{agg}(I))$ for votes from leaf nodes and then send an aggregate to the root.

For conditions (Tb) and (Tb'), a correct root will either: (1) suspect one of the intermediate nodes based on (Ta'), (2) receive $u + 1$ suspicions on leaf nodes, or (3) collect and forwards a quorum of votes in time to prevent intermediate nodes from triggering (Tb).

In cases (1) and (2) above, where the root collects or issues suspicions, the intermediate not will not trigger case (Tb).

Similarly, a correct leaf will receive suspicions from a correct root before triggering (Tb'). Finally, a correct intermediate node will either forward proposals to the leaf or broadcast a suspicion against the root before triggering (Tb').

If no suspicions are raised due to timeouts, condition (Tc) will not be triggered either. \square

To prove our main theorem, about the number of reconfigurations needed to find a correct tree, we consider new subsets $\mathcal{E}_d^n \subset \mathcal{E}_d$, $\mathcal{T}^n \subset \mathcal{T}$, and $\mathcal{C}^n \subset \mathcal{C}$ which are added to the respective sets after GST. [Lemma 4](#) shows that the size of these data-structures reflects the number of faulty replicas removed from the candidate set. [Lemma 2](#) shows that for any two failed trees, the size of these data-structures increases by at least one. [Lemmas 6](#) and [7](#) show that other mechanisms do not reduce the size. We denote the total size of these structures as $t^n = |\mathcal{C}^n| + |\mathcal{E}_d^n| + |\mathcal{T}^n|$.

Lemma 4. If $t^n = t$, then a working configuration is found.

Proof. After GST, no two correct replicas raise suspicions on each other and all suspicions on correct replicas are reciprocated. Therefore, if a replica was added to \mathcal{C}^n it is indeed faulty. Further, if a new edge was added to \mathcal{G} , then at least one of the adjacent replicas is faulty. Thus, for every edge in \mathcal{E}_d^n , at least one of the adjacent nodes is faulty, and for each triangle build from a replica in \mathcal{T}^n and an edge in \mathcal{E}_d^n ,

at least two of the adjacent replicas are faulty. Finally, for a triangle in \mathcal{G} containing a replica in \mathcal{T}^n and an edge in \mathcal{E}_d but not in \mathcal{E}_d^n , at least one of the adjacent replicas is faulty. Thus t^n many faulty replicas have been removed from the candidate set for internal nodes. \square

Lemma 5. If a tree failed after GST, either: (i) $|\mathcal{E}_d^n|$ increases, or (ii) $|\mathcal{T}^n|$ increases and $|\mathcal{E}_d^n|$ stays unchanged. Also, either t' increases, or t' stays constant and \mathcal{T}^n decreases.

This Lemma is a variation of Lemma 2 and the proof follows the same schema.

Proof. All suspicions are added to the graph \mathcal{G} . In case (1) of Lemma 1, the new suspicion can be added to \mathcal{E}_d^n and \mathcal{T} remains unchanged, increasing t' . In case (2), $u + 1$ edges are added to \mathcal{G} . These new edges include $u + 1$ different leaves from the failed tree. These leaves, can be already adjacent to an edge in \mathcal{E}_d or part of \mathcal{T} . There are three cases: a) one leaf was not part of \mathcal{E}_d or \mathcal{T} . The new edge can be added to \mathcal{E}_d^n giving case (i) of the Lemma. b) one leaf was part of \mathcal{T} . The new edge can be added to \mathcal{E}_d^n and $|\mathcal{T}|$, possibly also $|\mathcal{T}^n|$ is reduced by 1, giving case (ii) of the Lemma. In this case, t' stays constant. (3) all leaves are part of \mathcal{E}_d , but since $|\mathcal{E}_d| \leq u$, at least two suspected leaves are already connected in \mathcal{E}_d . This allows to either replace one edge in \mathcal{E}_d by two in \mathcal{E}_d^n , or add a new node to \mathcal{T}^n . Also here t' increases. \square

If a new suspicion is raised between two nodes in G , it is first treated as a two way suspicion and added to \mathcal{G} . If no reciprocation happens during the next $f + 1$ views, then the suspected replica is added to C . The next Lemma proves that these changes do not decrease t' .

Lemma 6. If nodes are added to C due to not reciprocated suspicions, this does not change t' , and does not increase \mathcal{T}^n .

Proof. Clearly, if an edge is removed from \mathcal{E}_d^n , then a replica is added to C^n . In some cases the removal removing an edge from \mathcal{E}_d causes that a replica is removed from \mathcal{T}^n and instead, a new edge is added to \mathcal{E}_d^n . Thus t' does not change. \square

All suspicions added after GST include at least one faulty replica. Thus these suspicions leave an independent set of $n - f$ correct replicas. However, suspicions made before GST may be successively removed after GST.

Lemma 7. If suspicions made before GST are discarded, removing replicas from C , or removing edges from \mathcal{G} , t' does not decrease, and \mathcal{T}^n does not increase.

Proof. Clearly this does not reduce C^n and \mathcal{E}_d^n . However, if an edge in \mathcal{E}_d is removed, it can be that a replica in \mathcal{T}^n is no longer part of a triangle. However, the replica in \mathcal{T}^n is adjacent to an edge added after GST. This edge can now be added to \mathcal{E}_d^n , leaving t' unchanged. \square

Theorem 6.2. After GST, SmartTree finds a working configuration after at most $2t$ reconfigurations.

Proof. Based on Lemma 4, we only have to show that after $2t$ reconfigurations, $t' = t$. According to Lemma 2, after a reconfiguration, either t' increases, or t' stays constant and \mathcal{T}^n decreases. Since \mathcal{T}^n can only decrease by k after \mathcal{T}^n and t' have been increased by k . Thus at most t' reconfigurations can leave t' unchanged. \square

7 Related Work

Several prior works [41, 55] use accountability as a tool to enhance security by supporting forensics to identify misbehaving replicas. PeerReview [28] introduced a comprehensive method to establish accountability in distributed systems by auditing messages from other replicas. However, due to the extensive message exchange among replicas, this approach may be too costly for RSMs. Polygraph [14] introduced accountable Byzantine agreement by logging protocol messages to justify the decisions made by replicas. IA-CCF [46] improves on Polygraph by providing individual accountability through the use of *ledgers* and *receipts*. It relies on trusted execution environments to secure replicas. Given a set of conflicting receipts and a ledger, any third party can generate proof-of-misbehavior against at least $n/3$ replicas. SmartLog, however, does not require logging all protocol messages to ensure accountable configurations. Instead, it captures and records the underlying metrics involved in system configuration decisions. Moreover, SmartLog's flexible architecture can support sensor-monitor pairs to provide even stronger accountability if needed.

Kauri [42] uses random partitions to create a tree topology for scaling BFT protocols. While random selection offers a probabilistically working tree, these trees can suffer from poor performance. Several previous works [18, 37, 39] have optimized configuration latency by selecting leaders based on location. Other approaches [9, 44, 48] rank configurations to identify the optimal one. Wheat [48] assumes a topology-aware configuration, relying on external systems for replica monitoring and weight-vote allocation during view changes, which may not align with the BFT trust model. Aware [9] improves on Wheat by globally logging latency measurements to compute the weight-vote assignment deterministically. However, these mechanisms provide limited accountability and focus more on optimizing configurations than selecting a working configuration. SmartLog takes a comprehensive approach to select a working configuration within a fixed number of reconfigurations, ensuring accountable decisions while supporting non-deterministic configuration methods.

Abstract [5] introduced a switching mechanism to enable more efficient protocols under favorable conditions and reverts to more resilient protocols when conditions deteriorate. Similarly, Dahlia et al. [52] propose a system to collect

and replicate configuration metrics and use them in a reinforcement learning-based mechanism to switch between protocols. Adapt [7] presents a quality control system that assesses the suitability of a configuration and protocol based on the current environment. While protocol switching is a useful fallback mechanism, these systems do not address the specific needs of RSM optimizations [10], such as committee selection, hierarchical consensus, and pipelining. SmartLog provides a flexible framework to log relevant measurements and use them to enhance such optimizations.

8 Conclusion

We show that RSM optimizations are difficult to maintain in a dynamically changing environment, especially in the presence of faulty replicas and potentially manipulated measurements. SmartLog’s sensors and monitors allow to collect local measurements and perform non-deterministic computations, and to present and process this information consistently. SmartLog allows to select candidates for special roles and hold faulty replicas accountable to the reported measurements. We showcase how SmartTree leverages SmartLog to find more performant configurations and to stay optimized despite failures. Especially, the estimate on actual faults in the system, provided by SmartLog, allows SmartTree to balance performance and robustness.

9 Acknowledgments

This work was partially funded by the BBChain project under grant 274451 from the Research Council of Norway. This work has also been funded by Deutsche Forschungsgemeinschaft (DFG, German Research Foundation) grant number 446811880 (BFT2Chain).

10 Notation

References

- [1] 2023. Etc. https://etcd.io/docs/v3.5/dev-guide/discovery_protocol/.
- [2] 2023. Etc. Tuning. <https://etcd.io/docs/v3.5/tuning/>.
- [3] Yair Amir, Brian Coan, Jonathan Kirsch, and John Lane. 2011. Prime: Byzantine Replication under Attack. *IEEE Transactions on Dependable and Secure Computing* 8, 4 (jul 2011), 564–577. <https://doi.org/10.1109/TDSC.2010.70>
- [4] James W. Anderson, Hein Meling, Alexander Rasmussen, Amin Vahdat, and Keith Marzullo. 2017. Local Recovery for High Availability in Strongly Consistent Cloud Services. *IEEE Transactions on Dependable and Secure Computing* 14, 2 (2017), 172–184. <https://doi.org/10.1109/TDSC.2015.2443781>
- [5] Pierre-Louis Aublin, Rachid Guerraoui, Nikola Knežević, Vivien Quéma, and Marko Vukolić. 2015. The Next 700 BFT Protocols. *ACM Transactions on Computer Systems* 32, 4, Article 12 (jan 2015), 45 pages. <https://doi.org/10.1145/2658994>
- [6] Pierre-Louis Aublin, Sonia Ben Mokhtar, and Vivien Quéma. 2013. RBFT: Redundant Byzantine Fault Tolerance. In *2013 IEEE 33rd International Conference on Distributed Computing Systems*. 297–306. <https://doi.org/10.1109/ICDCS.2013.53>
- [7] Jean-Paul Bahsoun, Rachid Guerraoui, and Ali Shoker. 2015. Making BFT Protocols Really Adaptive. In *2015 IEEE International Parallel and*

Notation	Description
n	total number of replicas in the configuration
q	number of replicas in a quorum
f	number of failures tolerated
t	actual faults in the configuration
u	estimate on number of non-crash faults in the configuration
b	branching factor of the tree
i	the number of internal nodes
w	window length for sliding window mechanism
k	number of nodes from which the tree’s root collects votes
A, B, C, D	replicas
R	root node of a tree
I	intermediate node of a tree
T	leaf node of a tree
L	leader node
A_t	a node in a triangle
B_c	a crashed node
S_1	sensor type 1
M_1	monitor type 1
Π	the full configuration with n replicas
Γ	a configuration proposal
C	set of crashed replicas
\mathcal{F}	set of provably faulty replicas
\mathcal{K}	set of replicas that are candidates for special roles
\mathcal{G}	suspicion graph
\mathcal{V}	set of vertices in \mathcal{G}
\mathcal{E}	set of edges in \mathcal{G}
Q	quorum of nodes in a configuration
τ	a tree
M	set of all intermediate nodes in a tree
I	set of all internal nodes in a tree
\mathcal{L}	set of all leaf nodes in a tree
IS	independent set of nodes
\mathcal{E}_d	maximal set of disjoint nodes with two-way suspicions
\mathcal{T}	set of nodes that form a triangle with two nodes in \mathcal{E}_d
$A \leftrightarrow B$	replica A suspects replica B
$L_r(A, B)$	recorded latency between replicas A and B
$L_d(A, B)$	actual latency between replicas A and B
$L_{agg}(I)$	time to aggregate votes at intermediate node I
$score(k, \tau)$	the minimum latency to collect votes from k nodes
L	latency matrix
$L_{A,B}$	latency matrix element between replicas A and B
δ	multiplier used in timer calculations

- [8] Omar Mohammed Bakr and Idit Keidar. 2008. *On the Performance of Quorum Replication on the Internet*. Technical Report UCB/EECS-2008-141. EECS Department, University of California, Berkeley. <http://www2.eecs.berkeley.edu/Pubs/TechRpts/2008/EECS-2008-141.html>
- [9] Christian Berger, Hans P. Reiser, Joao Sousa, and Alysso Bessani. 2022. AWARE: Adaptive Wide-Area Replication for Fast and Resilient Byzantine Consensus. *IEEE Transactions on Dependable and Secure Computing* 19, 3 (may 2022), 1605–1620. <https://doi.org/10.1109/tdsc.2020.3030605>
- [10] Christian Berger, Signe Schwarz-Rüsch, Arne Vogel, Kai Bleeke, Leander Jehl, Hans P. Reiser, and Rüdiger Kapitza. 2023. SoK: Scalability Techniques for BFT Consensus. In *IEEE International Conference on Blockchain and Cryptocurrency, ICBC 2023, Dubai, United Arab Emirates, May 1-5, 2023*. IEEE, 1–18. <https://doi.org/10.1109/ICBC56567.2023.10174976>

- [11] Alysson Bessani, João Sousa, and Eduardo E. P. Alchieri. 2014. State Machine Replication for the Masses with BFT-SMART. In *Proceedings of the 2014 44th Annual IEEE/IFIP International Conference on Dependable Systems and Networks (DSN '14)*. IEEE Computer Society, 355–362. <https://doi.org/10.1109/DSN.2014.43>
- [12] Ethan Buchman, Jae Kwon, and Zarko Milosevic. 2018. The latest gossip on BFT consensus. *CoRR* abs/1807.04938 (2018). arXiv:1807.04938 <http://arxiv.org/abs/1807.04938>
- [13] Miguel Castro and Barbara Liskov. 1999. Practical Byzantine Fault Tolerance. In *Proceedings of the Third Symposium on Operating Systems Design and Implementation* (New Orleans, Louisiana, USA) (*OSDI '99*). USENIX Association, 173–186.
- [14] Pierre Civi, Seth Gilbert, and Vincent Gramoli. 2021. Polygraph: Accountable Byzantine Agreement. In *2021 IEEE 41st International Conference on Distributed Computing Systems (ICDCS)*. 403–413. <https://doi.org/10.1109/ICDCS51616.2021.00046>
- [15] Jeffrey Dean and Sanjay Ghemawat. 2004. MapReduce: Simplified Data Processing on Large Clusters. In *OSDI'04: Sixth Symposium on Operating System Design and Implementation*. 137–150.
- [16] Sisi Duan, Karl N. Levitt, Hein Meling, Sean Peisert, and Haibin Zhang. 2014. ByzID: Byzantine Fault Tolerance from Intrusion Detection. In *33rd IEEE International Symposium on Reliable Distributed Systems, SRDS 2014, Nara, Japan, October 6-9, 2014*. IEEE Computer Society, 253–264. <https://doi.org/10.1109/SRDS.2014.28>
- [17] Cynthia Dwork, Nancy Lynch, and Larry Stockmeyer. 1988. Consensus in the Presence of Partial Synchrony. *J. ACM* 35, 2 (apr 1988), 288–323. <https://doi.org/10.1145/42282.42283>
- [18] Michael Eischer and Tobias Distler. 2018. Latency-Aware Leader Selection for Geo-Replicated Byzantine Fault-Tolerant Systems. In *2018 48th Annual IEEE/IFIP International Conference on Dependable Systems and Networks Workshops (DSN-W)*. 140–145. <https://doi.org/10.1109/DSN-W.2018.00053>
- [19] Michael Eischer, Benedikt Straßner, and Tobias Distler. 2020. Low-Latency Geo-Replicated State Machines with Guaranteed Writes (*PaPoC '20*). ACM, Article 13, 9 pages. <https://doi.org/10.1145/3380787.3393686>
- [20] Vitor Enes, Carlos Baquero, Tuanir França Rezende, Alexey Gotsman, Matthieu Perrin, and Pierre Sutra. 2020. State-Machine Replication for Planet-Scale Systems. In *Proceedings of the Fifteenth European Conference on Computer Systems* (Heraklion, Greece) (*EuroSys '20*). ACM, Article 24, 15 pages. <https://doi.org/10.1145/3342195.3387543>
- [21] Yossi Gilad, Rotem Hemo, Silvio Micali, Georgios Vlachos, and Nickolai Zeldovich. 2017. Algorand: Scaling Byzantine Agreements for Cryptocurrencies (*SOSP '17*). ACM, 51–68. <https://doi.org/10.1145/3132747.3132757>
- [22] Neil Giridharan, Florian Suri-Payer, Matthew Ding, Heidi Howard, Ittai Abraham, and Natacha Crooks. 2023. BeeGees: Stayin' Alive in Chained BFT. In *Proceedings of the 2023 ACM Symposium on Principles of Distributed Computing* (Orlando, FL, USA) (*PODC '23*). ACM, 233–243. <https://doi.org/10.1145/3583668.3594572>
- [23] Guy Golan Gueta, Ittai Abraham, Shelly Grossman, Dahlia Malkhi, Benny Pinkas, Michael Reiter, Dragos-Adrian Seredinschi, Orr Tamir, and Alin Tomescu. 2019. SBFT: A Scalable and Decentralized Trust Infrastructure. In *2019 49th Annual IEEE/IFIP International Conference on Dependable Systems and Networks (DSN)*. 568–580. <https://doi.org/10.1109/DSN.2019.00063>
- [24] Krishna P. Gummedi, Stefan Saroiu, and Steven D. Gribble. 2002. King: Estimating Latency between Arbitrary Internet End Hosts. In *Proceedings of the 2nd ACM SIGCOMM Workshop on Internet Measurement* (Marseille, France) (*IMW '02*). ACM, 5–18. <https://doi.org/10.1145/637201.637203>
- [25] Bingyong Guo, Zhenliang Lu, Qiang Tang, Jing Xu, and Zhenfeng Zhang. 2020. Dumbo: Faster Asynchronous BFT Protocols. In *Proceedings of the 2020 ACM SIGSAC Conference on Computer and Communications Security* (Virtual Event, USA) (*CCS '20*). ACM, 803–818. <https://doi.org/10.1145/3372297.3417262>
- [26] Suyash Gupta, Jelle Hellings, and Mohammad Sadoghi. 2021. RCC: Resilient Concurrent Consensus for High-Throughput Secure Transaction Processing. In *2021 IEEE 37th International Conference on Data Engineering (ICDE)*. 1392–1403. <https://doi.org/10.1109/ICDE51399.2021.00124>
- [27] Andreas Haeberlen, Petr Kouznetsov, and Peter Druschel. 2006. The Case for Byzantine Fault Detection. In *Proceedings of the 2nd Conference on Hot Topics in System Dependability - Volume 2* (Seattle, WA) (*HOTDEP'06*). USENIX Association, 5.
- [28] Andreas Haeberlen, Petr Kouznetsov, and Peter Druschel. 2007. Peer-Review: Practical Accountability for Distributed Systems. In *Proceedings of Twenty-First ACM SIGOPS Symposium on Operating Systems Principles* (Stevenson, Washington, USA) (*SOSP '07*). ACM, 175–188. <https://doi.org/10.1145/1294261.1294279>
- [29] Patrick Hunt, Mahadev Konar, Flavio P. Junqueira, and Benjamin Reed. 2010. ZooKeeper: Wait-free Coordination for Internet-scale Systems. In *2010 USENIX Annual Technical Conference (USENIX ATC 10)*. USENIX Association. <https://www.usenix.org/conference/usenix-atc-10/zookeeper-wait-free-coordination-internet-scale-systems>
- [30] Mohammad M. Jalalzai, Costas Busch, and Golden G. Richard. 2019. Proteus: A Scalable BFT Consensus Protocol for Blockchains. In *2019 IEEE International Conference on Blockchain (Blockchain)*. 308–313. <https://doi.org/10.1109/Blockchain.2019.00048>
- [31] Leander Jehl. 2019. Quorum selection for Byzantine fault tolerance. In *2019 IEEE 39th International Conference on Distributed Computing Systems (ICDCS)*. IEEE, 2168–2177.
- [32] S. Kirkpatrick, C. D. Gelatt, and M. P. Vecchi. 1983. Optimization by Simulated Annealing. *Science* 220, 4598 (1983), 671–680. <https://doi.org/10.1126/science.220.4598.671> arXiv:<https://www.science.org/doi/pdf/10.1126/science.220.4598.671>
- [33] Marios Kogias and Edouard Bugnion. 2020. HovercRaft: Achieving Scalability and Fault-Tolerance for Microsecond-Scale Datacenter Services. In *Proceedings of the Fifteenth European Conference on Computer Systems* (Heraklion, Greece) (*EuroSys '20*). ACM, Article 25, 17 pages. <https://doi.org/10.1145/3342195.3387545>
- [34] Eleftherios Kokoris-Kogias, Philipp Jovanovic, Nicolas Gailly, Ismail Khoffi, Linus Gasser, and Bryan Ford. 2016. Enhancing Bitcoin Security and Performance with Strong Consistency via Collective Signing. In *Proceedings of the 25th USENIX Conference on Security Symposium* (Austin, TX, USA) (*SEC'16*). USENIX Association, 279–296.
- [35] Eleftherios Kokoris-Kogias, Philipp Jovanovic, Linus Gasser, Nicolas Gailly, Ewa Syta, and Bryan Ford. 2018. OmniLedger: A Secure, Scale-Out, Decentralized Ledger via Sharding. In *2018 IEEE Symposium on Security and Privacy (SP)*. 583–598. <https://doi.org/10.1109/SP.2018.000-5>
- [36] Ramakrishna Kotla, Lorenzo Alvisi, Mike Dahlin, Allen Clement, and Edmund Wong. 2010. Zyzzyva: Speculative Byzantine Fault Tolerance. *ACM Transactions on Computer Systems* 27, 4, Article 7 (jan 2010), 39 pages. <https://doi.org/10.1145/1658357.1658358>
- [37] Shengyun Liu and Marko Vukolić. 2017. Leader Set Selection for Low-Latency Geo-Replicated State Machine. *IEEE Transactions on Parallel and Distributed Systems* 28, 7 (2017), 1933–1946. <https://doi.org/10.1109/TPDS.2016.2636148>
- [38] Shengyun Liu, Wenbo Xu, Chen Shan, Xiaofeng Yan, Tianjing Xu, Bo Wang, Lei Fan, Fuxi Deng, Ying Yan, and Hui Zhang. 2023. Flexible Advancement in Asynchronous BFT Consensus. In *Proceedings of the 29th Symposium on Operating Systems Principles* (Koblenz, Germany) (*SOSP '23*). ACM, 264–280. <https://doi.org/10.1145/3600006.3613164>

- [39] Yanhua Mao, Flavio P. Junqueira, and Keith Marzullo. 2008. Mencius: Building Efficient Replicated State Machines for WANs. In *Proceedings of the 8th USENIX Conference on Operating Systems Design and Implementation* (San Diego, California) (OSDI'08). USENIX Association, 369–384.
- [40] Michael G. Merideth, Florian Oprea, and Michael K. Reiter. 2009. When and How to Change Quorums on Wide Area Networks. In *2009 28th IEEE International Symposium on Reliable Distributed Systems*. 12–21. <https://doi.org/10.1109/SRDS.2009.35>
- [41] Nikolaos Michalakis, Robert Soulé, and Robert Grimm. 2007. Ensuring Content Integrity for Untrusted Peer-to-Peer Content Distribution Networks. In *4th USENIX Symposium on Networked Systems Design & Implementation (NSDI 07)*. USENIX Association. <https://www.usenix.org/conference/nsdi-07/ensuring-content-integrity-untrusted-peer-peer-content-distribution-networks>
- [42] Ray Neiheiser, Miguel Matos, and Luís Rodrigues. 2021. Kauri: Scalable BFT Consensus with Pipelined Tree-Based Dissemination and Aggregation. In *Proceedings of the ACM SIGOPS 28th Symposium on Operating Systems Principles* (Virtual Event, Germany) (SOSP '21). ACM, 35–48. <https://doi.org/10.1145/3477132.3483584>
- [43] Shota Numakura, Junya Nakamura, and Ren Ohmura. 2019. Evaluation and Ranking of Replica Deployments in Geographic State Machine Replication. In *2019 38th International Symposium on Reliable Distributed Systems Workshops (SRDSW)*. 37–42. <https://doi.org/10.1109/SRDSW49218.2019.00014>
- [44] Shota Numakura, Junya Nakamura, and Ren Ohmura. 2019. Evaluation and Ranking of Replica Deployments in Geographic State Machine Replication. In *2019 38th International Symposium on Reliable Distributed Systems Workshops (SRDSW)*. 37–42. <https://doi.org/10.1109/SRDSW49218.2019.00014>
- [45] Peter Pacheco. 1996. *Parallel Programming with MPI*. Morgan Kaufmann.
- [46] Alex Shamis, Peter Pietzuch, Burcu Canakci, Miguel Castro, Cedric Fournet, Edward Ashton, Amaury Chamayou, Sylvan Clebsch, Antoine Delignat-Lavaud, Matthew Kerner, Julien Maffre, Olga Vrousseau, Christoph M. Wintersteiger, Manuel Costa, and Mark Russinovich. 2022. IA-CCF: Individual Accountability for Permissioned Ledgers. In *19th USENIX Symposium on Networked Systems Design and Implementation (NSDI 22)*. USENIX Association, 467–491. <https://www.usenix.org/conference/nsdi22/presentation/shamis>
- [47] Peiyao Sheng, Gerui Wang, Kartik Nayak, Sreeram Kannan, and Pramod Viswanath. 2021. BFT Protocol Forensics. In *Proceedings of the 2021 ACM SIGSAC Conference on Computer and Communications Security* (Virtual Event, Republic of Korea) (CCS '21). ACM, 1722–1743. <https://doi.org/10.1145/3460120.3484566>
- [48] João Sousa and Alysson Bessani. 2015. Separating the WHEAT from the Chaff: An Empirical Design for Geo-Replicated State Machines. In *2015 IEEE 34th Symposium on Reliable Distributed Systems (SRDS)*. 146–155. <https://doi.org/10.1109/SRDS.2015.40>
- [49] Chrysoula Stathakopoulou, Tudor David, Matej Pavlovic, and Marko Vukolić. 2022. [Solution] Mir-BFT: Scalable and Robust BFT for Decentralized Networks. *Journal of Systems Research* 2, 1 (2022). <https://doi.org/10.5070/SR32159278>
- [50] Chrysoula Stathakopoulou, Matej Pavlovic, and Marko Vukolić. 2022. State Machine Replication Scalability Made Simple. In *Proceedings of the Seventeenth European Conference on Computer Systems* (Rennes, France) (EuroSys '22). ACM, 17–33. <https://doi.org/10.1145/3492321.3519579>
- [51] Pasindu Tennage, Cristina Basescu, Lefteris Kokoris-Kogias, Ewa Syta, Philipp Jovanovic, Vero Estrada-Galinanes, and Bryan Ford. 2023. QuePaxa: Escaping the Tyranny of Timeouts in Consensus. In *Proceedings of the 29th Symposium on Operating Systems Principles* (Koblenz, Germany) (SOSP '23). ACM, 281–297. <https://doi.org/10.1145/3600006.3613150>
- [52] Chenyuan Wu, Haoyun Qin, Mohammad Javad Amiri, Boon Thau Loo, Dahlia Malkhi, and Ryan Marcus. 2024. Towards Truly Adaptive Byzantine Fault-Tolerant Consensus. *SIGOPS Oper. Syst. Rev.* 58, 1 (Aug. 2024), 15–22. <https://doi.org/10.1145/3689051.3689055>
- [53] Maofan Yin, Dahlia Malkhi, Michael K. Reiter, Guy Golan Gueta, and Ittai Abraham. 2019. HotStuff: BFT Consensus with Linearity and Responsiveness. In *Proceedings of the 2019 ACM Symposium on Principles of Distributed Computing* (Toronto ON, Canada) (PODC '19). ACM, 347–356. <https://doi.org/10.1145/3293611.3331591>
- [54] Bin Yu, Joseph Liu, Surya Nepal, Jiangshan Yu, and Paul Rimba. 2019. Proof-of-QoS: QoS Based Blockchain Consensus Protocol. *Computers & Security* 87, C (nov 2019). <https://doi.org/10.1016/j.cose.2019.101580>
- [55] Aydan R. Yumerefendi and Jeffrey S. Chase. 2004. Trust but Verify: Accountability for Network Services. In *Proceedings of the 11th Workshop on ACM SIGOPS European Workshop* (Leuven, Belgium) (EW 11). ACM, 37–es. <https://doi.org/10.1145/1133572.1133585>
- [56] Matei Zaharia, Mosharaf Chowdhury, Tathagata Das, Ankur Dave, Justin Ma, Murphy McCauley, Michael J. Franklin, Scott Shenker, and Ion Stoica. 2012. Resilient Distributed Datasets: A Fault-Tolerant Abstraction for in-Memory Cluster Computing. In *Proceedings of the 9th USENIX Conference on Networked Systems Design and Implementation* (San Jose, CA) (NSDI'12). USENIX Association, 2.